Scaling Up of a Photoreactor for Formic Acid Degradation Employing Hydrogen Peroxide and UV Radiation

by **Marisol D. Labas**[1]), **Cristina S. Zalazar**[1]), **Rodolfo J. Brandi**[2]), **Carlos A. Martín**[3]), and **Alberto E. Cassano***[2])

Instituto de Desarrollo Tecnológico para la Industria Química, Universidad Nacional del Litoral and *CONICET*, Güemes 3450, (3000) Santa Fe, Argentina (Phone: +54-342-4559175/76/77; fax: +54-342-4559185; e-mail: acassano@intec.unl.edu.ar)

Dedicated to Professor *André M. Braun* on the occasion of his 60th birthday

A model for scaling up a homogeneous photoreactor was developed and experimentally verified in a pilot-plant-size apparatus. The procedure is exemplified by the oxidation of dilute aqueous HCOOH solutions with UV radiation (254 nm) and H_2O_2. First, the kinetic model and the kinetic parameters of the HCOOH degradation were obtained in a well-stirred, small, batch flat-plate photoreactor (volume = 70 ml). The method employed in the analysis of the experimental results yielded reaction-rate expressions for HCOOH and H_2O_2 that were independent of the reactor configuration. These kinetic equations and the corresponding kinetic constants were then used in a mathematical, fully deterministic model of a continuous-flow, 2-m-long, annular reactor (0.0065 m^2 of cross section for flow) operating in a laminar-flow regime to predict exit concentrations of HCOOH. Irradiation was provided in both cases by two different types of germicidal lamps. No additional experiments were made to adjust the reactor-model parameters. Theoretical predictions from the representation of the reactor performance obtained were compared with experimental data furnished by experiments in the much-larger-size, cylindrical-flow reactor. Results showed good agreement for the range of variables explored; they corresponded to expected operating conditions in water streams polluted with low concentrations of organic compounds.

1. Introduction. – One of the most powerful methods for designing a commercial-scale photoreactor is the use of rigorous mathematical modeling supported by properly analyzed laboratory experiments carried out in small reactors. When this procedure is correctly used, in many cases, it is possible to proceed directly from the laboratory size to the larger scale avoiding costly and time-consuming intermediate steps. Advanced oxidation technologies are not an exception, and developing methods for scaling up and designing these operations should greatly improve the spread of many of these new processes employed for air- and water-pollution treatment.

In photochemical reactors, radiation-field nonuniformities in the reaction space are irreducible. The participative characteristic of the reacting medium existing in the reactor volume (*i.e.*, the interaction of all species concentrations with the spatial distribution of available photons) strongly influences the rates. Thus, one of the best ways to produce a *one-step* extrapolation from the laboratory scale to any other reactor size consists in modeling both the small and the large reactor. In both cases, mass and

---

[1]) Fellowship holder from *CONICET*.

[2]) Research staff member from *CONICET* and Professor at UNL.

[3]) Research staff member from *CONICET*.

radiation balances are always needed. Under nonisothermal conditions, the thermal-energy balance will also be required, but this is not the case for the type of problems we are dealing with in the present work. In all but photosensitized or purely photocatalytic reactions (*i.e.*, reactions where direct photolysis is absent), all these balances will be coupled due to the changing concentration of the radiation-absorbing species. Fortunately, since the hydrogen peroxide/UV process is homogeneous, no scattering will be present.

Formic acid (HCOOH) has been used as model compound for degradation reactions on several occasions. Direct photolysis employing a medium-pressure Hg lamp with radiation below 250 nm has been reported by *Matsuura* and *Smith* [1]. Product distribution in the photo-oxidation reaction with H_2O_2 was studied by *Ogata et al.* [2], while pH effects on the same reaction were investigated by *Kawaguchi* [3]. HCOOH has also been used in photocatalytic research [4][5]. This reaction is most suitable for modeling studies because HCOOH is very soluble in water, its vapor pressure at room temperature is relatively low, and the oxidation reaction does not produce stable intermediates.

In this work, with HCOOH in aqueous solution as a model compound, the decomposition reaction employing H_2O_2 and UV radiation was modeled on two different scales: a small-size laboratory reactor (photoreactor volume = 70 ml) and a larger-scale reactor, a 2.0-m-long, annular photoreactor having a cross-sectional area of 65 cm^2. The small reactor was used to obtain an intrinsic kinetic expression for the decomposition reaction. The larger one was used to validate model predictions with new, additional experiments.

2. Mass and Radiation-Energy Balances for Both Reactors. – The general mass-balance equation is given by *Eqn. 1* [6], where C_i is the molar concentration of component i, $\boldsymbol{x}$ is the position in the reaction space, t is the time, $\boldsymbol{N}_i$ is the molar flux of component i (in mol/$cm^2 \cdot s$), and $R_{\mathrm{Hom},i}$ is the homogeneous, molar reaction rate of component i (per unit reaction volume). *Eqn. 1* can be applied to both reactors. For the laboratory reactor, it will provide the exact method to interpret the experimental data. For the larger reactor, it provides the tool to predict the reactor performance. The reaction-rate term includes the effect of the absorbed radiation.

$$\underbrace{\frac{\partial C_i(\boldsymbol{x},t)}{\partial t}}_{\text{Accumulation}} + \underbrace{\boldsymbol{\nabla}\cdot\boldsymbol{N}_{\mathrm{i}}(\boldsymbol{x},t)}_{\substack{\text{All mass fluxes}\\ \text{(Convection and diffusion)}}} = \underbrace{R_{\mathrm{Hom},i}(\boldsymbol{x},t)}_{\substack{\text{Homogeneous}\\ \text{Reactions}}} \quad i = \mathrm{H_2O_2},\ \mathrm{HCOOH} \tag{1}$$

Since *Eqn. 1* is a point-valued function, we need the equivalent description for the distribution of photons within the reactor. In the absence of emission and scattering, the transport of photons in space is given by *Eqn. 2*, where $I_{\lambda,\Omega}$ is the monochromatic specific intensity for light of wavelength λ and the direction of propagation is defined by the unit vector $\boldsymbol{\Omega}$ (in units of einstein/$s \cdot cm^2 \cdot$ steradian $\cdot$ cm), s is the distance traveled by the radiation ray, $\boldsymbol{x}$ is the position in space (usually represented in the coordinates defined by the reactor geometry), Ω is the solid angle describing the divergence of rays about the direction of propagation of radiation bundles (usually represented with

spherical coordinates and having the units of steradians), and κ_λ is the absorption coefficient of the radiation absorbing species at wavelength λ (in units of 1/cm). This equation is three-dimensional; the one-dimensional version of this representation, having κ_λ expressed in terms of a linear dependence upon the radiation absorbing species concentration, is usually known as *Lambert-Beer* equation. Once more, this equation must be applied to the laboratory reactor and to the large-scale one. Since κ_λ is a function of the radiation-absorption-species concentration, under normal conditions *Eqn. 2 is coupled with Eqn. 1*, *i.e.*, they must be solved simultaneously.

$$\underbrace{\frac{\mathrm{d}I_{\lambda,\Omega}[(\boldsymbol{x},\Omega),t]}{\mathrm{d}s(\boldsymbol{x})}}_{\substack{\text{Changes in } I \text{ along}\\ \text{the distance } ds}} + \underbrace{[\kappa_\lambda[(\boldsymbol{x}),t]I_{\lambda,\Omega}[(\boldsymbol{x},\Omega),t]}_{\substack{\text{Radiation absorption}\\ \text{in } ds}} = 0 \tag{2}$$

When *Eqn. 2* is solved, we obtain monochromatic-specific intensities (photons of a given energy/unit normal cross-sectional area, unit solid angle about the direction propagation $\boldsymbol{\Omega}$, unit time, and unit wavelength interval). From these values, the monochromatic incident radiation G_λ (photons of a given energy/unit normal cross-sectional area, unit time, and unit frequency interval) and the monochromatic local volumetric rate of photon absorption by the i component $e^a_{i,\lambda}$ (photons of a given energy/unit reaction volume, unit time, and unit frequency interval) can be readily calculated according to *Eqns. 3* and *4*, respectively. The incident radiation, sometimes also called spherical irradiance, is the integration of all specific intensities over the solid angle of incidence for all possible directions of irradiation within the reaction space.

$$G_\lambda(\boldsymbol{x}, t) = \int_\Omega I_{\Omega\lambda}(\boldsymbol{x}, \Omega, t)\, \mathrm{d}\Omega \tag{3}$$

$$e^a_{i,\lambda}(\boldsymbol{x}, t) = \kappa_{i,\lambda}(\boldsymbol{x}, t)\, G_\lambda(\boldsymbol{x}, t) \tag{4}$$

3. Laboratory Reactor. – 3.1. *Employed Equipment.* To gather kinetic information suitable for scaling-up purposes, one needs a careful design of the laboratory reactor. As important as the knowledge of the species concentrations, the distribution of photons in the reaction space must be well-understood. Taking advantage of the unfortunately low light-absorption properties of H_2O_2, one can even try to minimize the spatial variations of the light intensity. This approach could provide a reactor that is almost isoactinic (*i.e.*, the spatial distribution of photons is almost uniform). When this is the case, the 'square root of the average of the photon-absorption rate' is almost equal to 'the average of the photon-absorption rate risen to the square root power' [7]. If this approach is possible (very often it is not) and the dependence upon the photon-absorption rate is not linear, estimation of the reaction parameters can be greatly simplified.

To have an approximation to the ideal reactor, a flat-plate-reactor configuration having a circular cross section was irradiated from both sides with two tubular lamps.

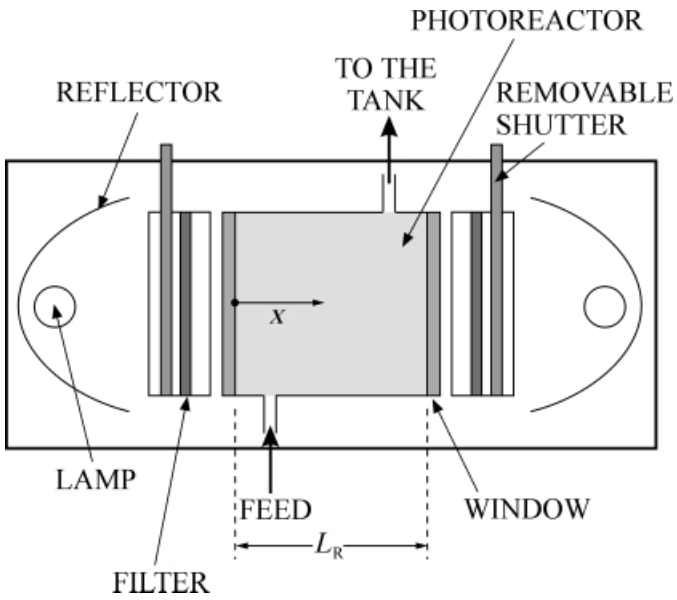

Fig. 1. *Flat plate reactor irradiated from both sides*

The lamps were placed at the focal axis of two cylindrical reflectors of parabolic cross section. Reflectors were made of an aluminium sheet, mirror polished by the *Alzac* treatment (*Fig. 1*). This particular geometry and the method used to irradiate the reactor facilitate the description of the radiation field, information that must be obtained even for the isoactinic case. The reactor (69.9 ml) was made of glass, while the flat windows were made of quartz plates (*Suprasil* quality). The reactor was part of a recycling system having an all-glass and *Teflon* storage tank (liquid volume = 2000 ml), provisions for maintaining the reaction temperature constant, and a recirculating pump (*Fig. 2*). The system as a whole operated in the batch mode with a high recirculating flow rate. Sampling was made in the tank. The incident flux of radiation on each reactor window was varied on three different levels: *i*) with a *Philips TUV* lamp (15 W each side), *ii*) with a *Heraeus UV-C* lamp (40 W each side), and *iii*) with a *Heraeus UV-C* lamp with an interposed neutral density filter on both sides. However, it must be noted that additional changes in the absorbed energy were produced by the different concentrations of H_2O_2 employed during experiments. Moreover, since the H_2O_2 concentration changed during the reaction, the local volumetric rate of photon absorption (LVRPA) in the reactor did so, too. Lamp operation was monitored with a *VAW* meter. Between the lamp-reflector system and the reactor, a removable shutter permitted operation of the reactor without irradiation and initiation of the reaction only after the lamps had reached the steady-state operation.

3.2. *Materials and Methods.* Three experimental variables were investigated: *1*) the concentration of HCOOH (*Merck*, PA-ACS), from 40 to 140 ppm, *2*) the molar ratio of H_2O_2 concentration (*Merck*, PA 30%) to HCOOH concentration, from 1.0 to 32, and *3*) the average value of the LVRPA at three different irradiation levels and several H_2O_2 concentrations. Distilled water was employed in all runs. The HCOOH concentration in

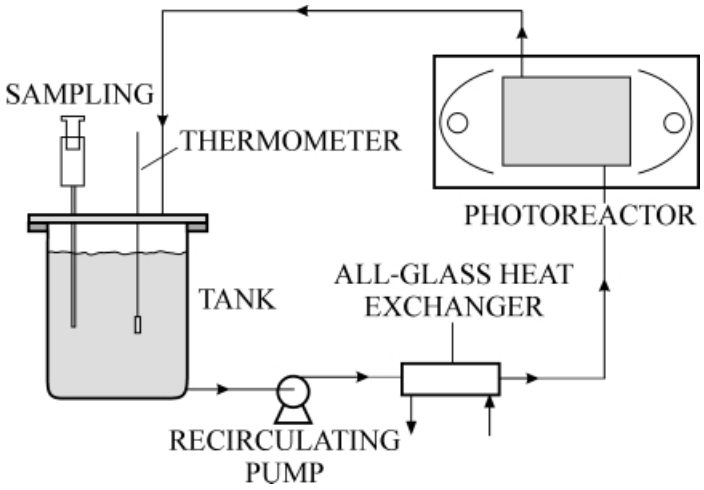

Fig. 2. *Experimental setup for kinetic studies*

water was determined with total-organic-carbon (*Shimadzu TOC-5000A*) and ion-chromatography (*Dionex 2020i*) measurements. H_2O_2 was analyzed by colorimetric methods [8] (*UV-vis-Cary-17-D* spectrophotometer). Additional experimental information was also collected: the optical characteristics (absorbance) of the reacting mixture were controlled in all samples.

In batch experiments, it is important to make sure that the equipment is operating under steady-state conditions for all parameters that are assumed to be constant, for example, lamp operation and temperature. Before starting each run, they were monitored for 1–2 h while a shutter was interposed between the lamps and the reactor. Only when steady-state conditions were reached, was the desired amount of H_2O_2 added to the mixture. The operating temp. was 20°. The reaction started when both shutters were removed. Samples (30 ml) were taken from the tank at specific time intervals for the different analysis.

3.3. *Modeling. Eqn. 1* will be applied to the recycling of the laboratory reactor. The following operating conditions must be fulfilled: *1*) the whole system operates under well-stirred conditions, *2*) the ratio of the reactor volume to the tank volume is <1 (even better when it is $\ll 1$), and *3*) the recirculating flow rate is high such as to have differential conversion per pass in the photoreactor. Under these conditions, it can be shown (*Appendix*) that the change in concentration in the tank is related to the reaction rate according to *Eqn. 5*, with the initial condition $C_i(t=0) = C_{i,0}$. The reaction rate is a function of position (x) because of the light distribution inside the reaction space. V_T is the total volume of the system and V_R is the volume of the photochemical reactor exclusively. Since irradiation by germicidal lamps is monochromatic, no integration over wavelengths is required; the symbol $\langle\ \rangle$ stands for a reactor volume averaged value. Note that this average is necessary because experimental measurements in the tank reflect the result produced by the *average* value of the reaction rate in the reactor volume.

$$\left.\frac{dC_i(t)}{dt}\right|_{\text{Tank}} = \frac{V_R}{V_T}\langle R_{\text{Hom},i,\lambda}(x,t)\rangle_{V_R}, \quad i = H_2O_2, \text{HCOOH} \tag{5}$$

In any kinetically controlled regime (*i.e.*, in the absence of mass-transport limitations), the photochemical reaction will depend on the radiation field inside the reactor. To obtain this information, *Eqn. 2* will be used. It has been shown that under some geometric restrictions (*i.e.*, conditions imposed on the equipment design that mainly involve distances and dimensions), the radiation field produced by the tubular lamp and the parabolic reflector can be modeled by one-dimensional representations [9–11]. When this is the case, in homogeneous systems, incident radiation and radiation intensities are equivalent concepts. As derived in [12], the incident radiation at any point x inside the reactor is given by the contributions of both lamps and expressed by *Eqn. 6*, where G_λ is the incident radiation at any point x, $G_{w,\lambda}$ is the incident radiation at the reactor wall (at $x=0$ and $x=L_R$), $\kappa_{j,\lambda}$ is the absorption coefficient of component j and L_R is the reactor length along the direction x. The local volumetric rate of photon absorption by component i is then given by *Eqn. 7*, where $e^a_{i\lambda}$ is the local volumetric rate of photon absorption (the LVRPA). If, as it is our case, absorption by formic acid at 254 nm is almost negligible, then $i=j=H_2O_2$. The value of $G_{w,\lambda}$ can be calculated from an emission model [9–11] or experimentally determined with potassium ferrioxalate actinometry [13]. The value of κ_λ for H_2O_2 at 254 nm and as a function of H_2O_2 concentration can be obtained spectroscopically and has been frequently reported in the literature. For low H_2O_2 concentrations, the absorption coefficient is obtained from the value of the molar naperian absorptivity (α_i) by application of *Beer*'s equation ($\kappa_{i,\lambda}=\alpha_{i,\lambda}C_i$).

$$G_\lambda(x,t)=G_{w,\lambda}\left\{\exp\left[-\left(\sum_j \kappa_{j,\lambda}(t)\right)x\right]+\exp\left[-\left(\sum_j \kappa_{j,\lambda}(t)\right)(L_R-x)\right]\right\};\ j=1,2,\ldots \quad (6)$$

$$e^a_{i,\lambda}(x,t)=\kappa_{i,\lambda}\,G_{w,\lambda}\left\{\exp\left[-\left(\sum_j \kappa_{j,\lambda}(t)\right)x\right]+\exp\left[-\left(\sum_j \kappa_{j,\lambda}(t)\right)(L_R-x)\right]\right\} \quad (7)$$

3.4. *Kinetic Model*. For design purposes, the best starting point to obtain a kinetic model is a known and well-established *reaction mechanism*. Generally, and unfortunately, this is not possible for a large group of reactions. The opposite case – corresponding to the maximum state of ignorance on possible reaction paths – is the proposal of a purely empirical kinetics. In between, it is always possible to use a plausible *reaction sequence*. Then, according to the experimental results obtained, it is conceivable to derive an equation that can be useful for representing, with a reasonable degree of approximation, the reaction evolution. We know from our experiments that the photo-oxidation of low concentrations of HCOOH has shown the following characteristics: *i*) the kinetics of HCOOH disappearance is independent of the HCOOH concentration but bears some relationship to the H_2O_2 concentration, *ii*) the O_2 concentration, within the limits of investigated variables, does not seem to affect the rate, *iii*) the H_2O_2 degradation is a function of its concentration, and the dependence is not strictly first order, and *iv*) the rate of disappearance of both compounds depends almost linearly upon the photon-absorption rate. The reaction sequence shown in *Eqn. 8* is proposed [14–16].

$$\begin{array}{lcll} H_2O_2 + h\nu & \rightarrow & 2\ OH^{\cdot} & \phi \\ H_2O_2 + OH^{\cdot} & \rightarrow & HO_2^{\cdot} + H_2O & k_2 \\ HO_2^{\cdot} + OH^{\cdot} & \rightarrow & H_2O + O_2 & k_3 \\ HO_2^{\cdot} + HO_2^{\cdot} & \rightarrow & H_2O_2 + O_2 & k_4 \\ HO_2^{\cdot} + H_2O_2 & \rightarrow & H_2O + O_2 + OH^{\cdot} & k_5 \\ OH^{\cdot} + OH^{\cdot} & \rightarrow & H_2O_2 & k_6 \\ OH^{\cdot} + HCOOH + O_2 & \rightarrow\rightarrow & CO_2 + H_2O + HO_2^{\cdot} & k_7 = k_7^{'}\ C_{O_2} \end{array} \quad (8)$$

Applying the local o micro steady-state approximation and considering that *1*) no square-root dependence with the LVRPA has been observed, *2*) $k_3 \gg k_4$, *3*) $k_5 \ll k_2$ and k_7, and *4*) $k_2 \cdot C_P/k_6 \cdot C_F \leq$ order 0.1, the approximate kinetic model of *Eqns. 9* and *10* can be readily obtained, where k_1^* and k_2^* are lumped kinetic constants and $r = C_{H_2O_2}/C_{HCOOH}$. According to *Eqns. 9* and *10*, only two parameters are needed to represent the kinetic model. These equations represent local values of the reaction rates (a function of x). To extract from experimental data the values of k_1^* and k_2^*, we must use *Eqn. 5*, which requires the average values of the reaction rates. In the well-mixed reactor, the radiation field is still not uniform, and, consequently, the reaction rate is a function of x and t. Hence, for the one-dimensional-radiation and reactor model, the average has to be calculated over the reactor length according to *Eqn. 11*. Numerical integration can be used in conjunction with the nonlinear parameter estimator. Parameters are obtained by matching predicted and experimental values of the *C vs. t* data. Predictions are obtained from *Eqns. 5*, *7*, and *9–11*.

$$R_{HCOOH}(x,t) = -\,k_1^*\ e_\lambda^a\ (x,t) \quad (9)$$

$$R_{H_2O_2}(x,t) = -\,k_2^*\ e_\lambda^a\ (x,t)\ r\ (t) \quad (10)$$

$$\langle R_{Hom,i}(x,t)\rangle_{V_R} = \langle R_{Hom,i}(x,t)\rangle_{L_R} \frac{1}{L_R} \int_0^{L_R} R_{Hom,i}\ (x,t)\ \mathrm{d}x \quad (11)$$

3.5. *Results*. The values for $G_{w,\lambda}$ for the three different experimental conditions were obtained with conventional actinometry. Experimental procedures based on potassium ferrioxalate actinometry were carried out according to *Murov et al.* [17]. Interpretation of the results was made with the procedure described by *Martín et al.* [13]. The resulting values are: $13.94 \cdot 10^{-9}$, $5.45 \cdot 10^{-9}$, and $2.33 \cdot 10^{-9}$ einstein/cm$^2 \cdot$ s. The molar absorptivity used for H_2O_2 at 254 nm was $0.368 \cdot 10^5$ cm^2/mol and $L_R = 4.9$ cm.

To verify the absence of dark reactions and of direct photolysis, two runs were carried out with HCOOH under the following conditions: with H_2O_2 and no UV radiation, and with no H_2O_2 and UV radiation, respectively. No significant changes in the HCOOH concentration were observed after 3 h.

Figs. 3 and *4* show results from two typical runs. Equivalent plots were obtained for twelve different runs within the previously described range of experimental variables. From the data and the kinetic model, with a nonlinear parameter estimator [18], the following lumped kinetic constants were obtained: $k_1^* = 0.3716 \pm 0.0114$ einstein/mol and $k_2^* = 0.0247 \pm 0.0087$ einstein/mol. Reported errors are for the 95% confidence interval. In *Figs. 3* and *4*, the solid lines correspond to values obtained with the kinetic

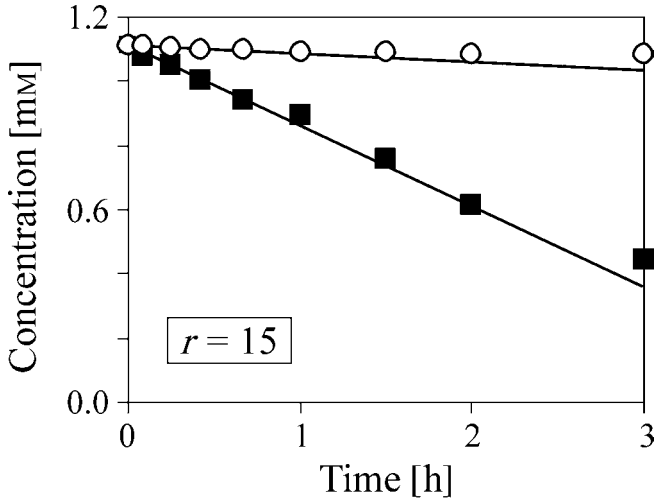

Fig. 3. *Results from a run in the flat-plate reactor with* r = *15*. ○: Experimental data for H_2O_2, ■: experimental data for HCOOH, —: kinetic model.

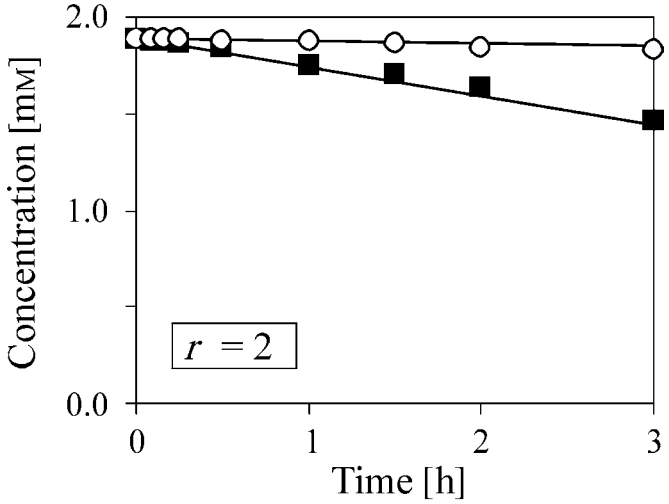

Fig. 4. *Results from a run in the flat-plate reactor with* r = *2*. ○: Experimental data for H_2O_2, ■: experimental data for HCOOH, —: kinetic model.

model and these two constants, *i.e.*, they do not correspond to direct fitting of the experimental data. The agreement in all cases is excellent. With these parameters, *Eqns. 9* and *10* can now be applied to the larger reactor.

4. Large Reactor. – 4.1. *Employed Equipment*. The employed apparatus is illustrated in *Fig. 5*. To use standard, commercial, low-priced germicidal lamps, the 2-m reactor was made of two sections of 1-m length connected in series, each 1-m-long reactor having an inner radius of 2.5 cm and an outer radius of 5.2 cm. Coaxial with

each annular space, a *Philips TUV-40* lamp (120 cm length, 2.6 cm in diameter) was placed, the lamp having a nominal input power of 40 W and an output of 12.6 W at 254 nm (0.105 W/cm). Although lamps with significant emission below 254 nm may be advisable (due to the low absorption of H_2O_2 at 254 nm), the present choice is not an obstacle for demonstrating the quality of the scale-up method. The reactor tubes and the lamp were properly positioned with custom-made *Teflon* ends. The reactor was fed with a stainless steel and *Viton* centrifugal pump that received the reaction mixture from a constant level tank. A second tank with pure water can be used to wash the reactor. Flow rates were controlled by acting electronically on the pump rotational speed and measured at the reactor exit line. Sampling was made between reactors and at the second reactor outlet.

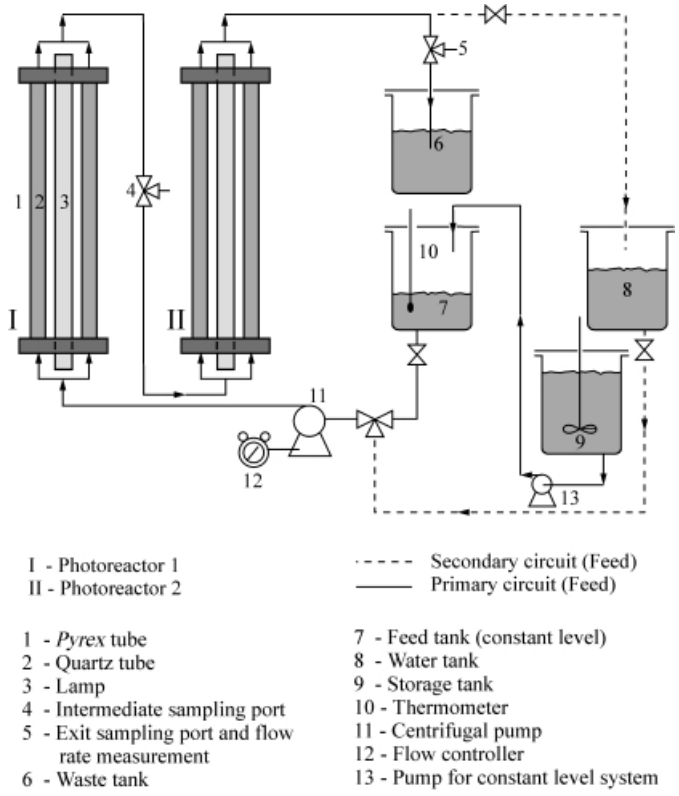

Fig. 5. *Large-scale-reactor setup*

4.2. *Materials and Methods.* The same reagents and analytic procedures as described in *Sect. 3.2* were used in the large-reactor operation. Each run started with the adjustment of flow rates and temp. for the reaction mixture; then, the light was turned on, and enough time was allowed to reach the steady state in the reactor operation. Measuring the exit concentration of HCOOH at both reactor exits permitted us to know whether the steady state was attained. After it was reached (depending on the flow rate, after *ca.* 30 min), the 'experimental output concentration' (to be compared with theoretical predictions from the model) was the result of the analysis of two more successive samples. Runs were made at different flow rates between 1 and 5 l/min, different initial HCOOH concentrations, and different $C_{H_2O_2}/C_{HCOOH}$ ratios.

4.3. *Modeling. Eqn. 1* will be applied to the tubular reactor under the following assumptions and operating conditions: *i*) steady state; *ii*) unidirectional, incompressible, continuous flow of a Newtonian fluid under fully developed laminar regime; *iii*) only ordinary diffusion is significant; *iv*) azimuthal symmetry, *v*) axial diffusion neglected as compared to the convective flow; *vi*) constant physical and transport properties. The model equation in cylindrical coordinates (r,z) is given by *Eqn. 12*, where v_z is the velocity distribution in the annular space (in cm/s), and D_{im} is the diffusivity of the i species in the mixture (in cm^2/s). This equation must be integrated with the initial and boundary conditions given in *Eqns. 13–14*, where $r_{R,i}$ and $r_{R,o}$ are, respectively, the inner and outer radii of the annular reactor. These boundary conditions state that the reactor wall is not permeable to mass fluxes. The velocity v_z can be obtained with a momentum balance with the same assumptions that were described for the mass balance. According to *Bird et al.* [6], *Eqn. 16* holds for the annular tube. Therein, ΔP is the pressure difference between inlet and outlet conditions (in dyne/cm^2), μ is the liquid viscosity (in g/cm s), L_R is the reactor length, and ϑ is the ratio of the inner and outer radii.

$$\underbrace{v_z(r)\frac{\partial C_i(z,r)}{\partial z}}_{\text{Convective flow in the axial direction}} - \underbrace{D_{im}\left[\frac{1}{r}\frac{\partial}{\partial r}\left(r\frac{\partial C_i(z,r)}{\partial r}\right)\right]}_{\text{Diffusional flux in the radial direction}} = \underbrace{R_{\text{Hom},i}(z,r)}_{\text{Homogeneous reaction rate}}, \quad i = H_2O_2, \text{HCOOH} \tag{12}$$

$$z = 0 \quad \text{and every } r \quad C_i = C_{i,0} \tag{13}$$

$$r = r_{R,i} \quad \text{and every } z \quad \frac{\partial C_i}{\partial r} = 0 \tag{14}$$

$$r = r_{R,o} \quad \text{and every } z \quad \frac{\partial C_i}{\partial r} = 0 \tag{15}$$

$$v_z(r) = \frac{\Delta P\, r_{R,o}^2}{4\mu L_R}\left[1 - \left(\frac{r}{r_{R,o}}\right)^2 + \left(\frac{1-\vartheta^2}{\ln(1/\vartheta)}\right)\ln\left(\frac{r}{r_{R,o}}\right)\right] \tag{16}$$

On the right-hand side of *Eqn. 12*, we must insert the results of the kinetic model, *i.e.*, *Eqns. 9* and *10* with the kinetic parameters obtained in the laboratory reactor. *Eqn. 12* with boundary and initial conditions of *Eqns. 13–15* must be solved numerically. Finite-difference techniques were used. The solution of the partial differential equation provides HCOOH and H_2O_2 exit concentrations as a function of the radial position. To compare these results with data from the actual reactor and considering the velocity distribution of the outgoing flow, the bulk or flow-average concentration must be calculated according to *Eqn. 17*.

$$C_{b,i} = \frac{\int_{r_{R,i}}^{r_{R,o}} v_z(r) C_i(r, z = L_R) r\, dr}{\int_{r_{R,i}}^{r_{R,o}} v_z(r) r\, dr} \tag{17}$$

As shown in the case of the small reactor, for using *Eqns. 9* and *10* in *Eqn. 12*, we need a model for the photon distribution in the annular space. It can be obtained with an emission model for the lamp, the optical characteristics of the reactor wall, the optical characteristics of the reaction space, and the geometric dimensions of the lamp-reactor system. *Fig. 6* shows the emission along the direction θ,ϕ produced by a small-volume element of the lamp that reaches the reactor at $s = s_R$. In view of *Fig. 6*, *Eqn. 2* can be integrated along this given direction of propagation (defined by the θ and ϕ coordinates) from $s = s_R$ (at an arbitrary point on the surface of radiation entrance to the reactor) to a point of incidence I_n inside the reactor, as expressed by *Eqn. 18*, where $I^0_\lambda(\theta,\phi,t) = I_\lambda(s_R,\Omega,t)$ is the boundary condition for I_λ at the point of entrance and for an arbitrary direction Ω. This boundary condition, provided by the lamp-emission model, has been developed by *Cassano et al.* [19], and has the value given in *Eqn. 19* for steady irradiation. Therein, $P_{s,\lambda}$ is the lamp output power at wavelength λ (photons per second), R_L is the lamp radius, L_L is the useful lamp length, and $Y_{R,\lambda}$ is a compounded transmission coefficient of the reactor wall (considering absorption and reflections).

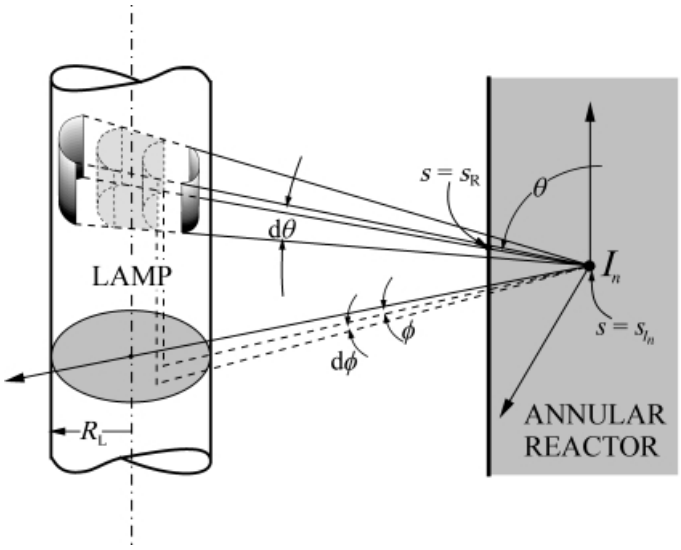

Fig. 6. *A model for emission by a tubular lamp along the direction θ,ϕ on a point* I_n *inside the annular reactor*

$$I_\lambda(x,\theta,\phi,t) = I^0_\lambda(\theta,\phi,t)\exp\left[-\int_{\bar{s}=s_R(x_0,\theta,\phi)}^{\bar{s}=s_I(x,\theta,\phi)} \kappa_{H_2O_2,\lambda}(\bar{s},t)\,d\bar{s}\right] \tag{18}$$

$$I^0_\lambda(\theta,\phi) = \frac{P_{S,\lambda}}{4\pi^2 R_L^2 L_L}\,\frac{(R_L^2 - r^2\sin^2\phi)^{1/2}}{\sin\phi}\,Y_{R,\lambda}(\theta,\phi) \tag{19}$$

Eqns. 18 and *19* give the radiation contribution of an arbitrary direction (θ,ϕ) to the point $I(x,\theta,\phi)$ inside the reactor. The next step is to integrate all possible directions of irradiation from the lamp volume of emission to the point I_n (*Fig. 7*). According to *Irazoqui et al.* [20], the value of the incident radiation (G_λ) at a point x inside the reactor is obtained by integration over the solid angle of incidence ($d\Omega = \sin\theta\, d\theta\, d\phi$) as shown in *Eqn. 20*. In the double integral, θ accounts for the lamp length and ϕ for the

lamp diameter. The integration limits are given by *Eqns. 21–23* [20]. Finally, at any point inside the annular reaction space, the LVRPA is expressed by *Eqn. 24*. The latter has to be inserted in *Eqns. 9* and *10* to provide the reaction rates for *Eqn. 12*. We have now all the necessary information to predict, after integration of *Eqn. 12*, the exit concentrations in the large reactor. It is obvious that integration must be done numerically.

$$G_\lambda(x,t) = \int_{\phi_1}^{\phi_2} \mathrm{d}\phi \int_{\theta_1(\phi)}^{\theta_2(\phi)} \mathrm{d}\theta \sin\theta I_\lambda^0(\theta,\phi) \exp\Big[-\int_{\bar{s}=s_R(x_0,\theta,\phi)}^{\bar{s}=s_l(x,\theta,\phi)} \kappa_{\mathrm{H_2O_2},\lambda}(\bar{s},t)\mathrm{d}\bar{s}\Big] \tag{20}$$

$$\theta_1(\phi) = \tan^{-1}\left\{\frac{r\cos\phi - [r^2(\cos^2\phi - 1) + R_\mathrm{L}^2]^{1/2}}{(\mathrm{L_L} - \mathrm{z})}\right\} \text{ top of the lamp} \tag{21}$$

$$\theta_2(\phi) = \tan^{-1}\left\{\frac{r\cos\phi - [r^2(\cos^2\phi - 1) + R_\mathrm{L}^2]^{1/2}}{-z}\right\} \text{ bottom of the lamp} \tag{22}$$

$$-\phi_1 = \phi_2 = \cos^{-1}\left[\frac{(r^2 - R_\mathrm{L}^2)^{1/2}}{r}\right] \tag{23}$$

$$e_\lambda^a(x,t) = \kappa_{\mathrm{H_2O_2},\lambda}(x,t) \int_{\phi_1}^{\phi_2} \mathrm{d}\phi \int_{\theta_1(\phi)}^{\theta_2(\phi)} \mathrm{d}\theta \sin\theta I_\lambda^0(\theta,\phi) \exp\Big[-\int_{\bar{s}=s_R(x_0,\theta,\phi)}^{\bar{s}=s_l(x,\theta,\phi)} \kappa_{\mathrm{H_2O_2},\lambda}(\bar{s},t)\mathrm{d}\bar{s}\Big] \tag{24}$$

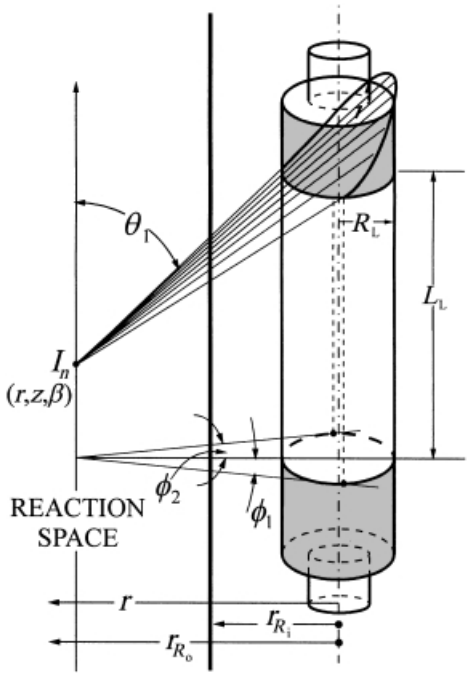

Fig. 7. *Limits for integration of the total lamp emission on a point inside the reactor*

4.4. *Results.* The data on the lamp emission provided by the manufacturer (0.105 W/cm) were verified by homogeneous actinometry. This type of experiments, performed with a reaction solution having strong absorption properties and properly analyzed, permits the correct evaluation of the boundary condition to be used in *Eqn. 24*. The corrected lamp output power was then introduced in *Eqn. 19*. Predictions obtained from *Eqns. 12–24* were compared with experimental conversions in terms of *Eqn. 25*. The *Table* shows results of three runs with the larger reactor. It can be seen that theoretical values show reasonably good agreement with the measured exit concentrations. It should be mentioned that results from the model were not subjected to any sort of empirical adjustment. These results confirm the validity of the kinetic model represented by *Eqns. 9* and *10* and the procedure used to calculate the corresponding kinetic constants (the precise modeling of the laboratory reactor). Moreover, it confirms the quality of calculated values of the lamp emission and radiation distribution inside the annular space (from the model). We think that the observed deviations are mainly due to the practical difficulties in having fully developed laminar flow at all (four) reactor ends (*i.e.*, certainly, *Eqn. 16* is not rigorously applicable to these reactors). It does not seem advisable to complicate the momentum balance to the extreme of including these perturbations.

$$x_{b,i} = \frac{C_{i,0} - C_{\mathrm{b},i}}{C_{i,0}} \quad i = \mathrm{H_2O_2},\ \mathrm{HCOOH} \tag{25}$$

Table. *Scale-Up: Prediction* vs. *Experiment*

Run	C_{HCOOH} [ppm]	*r*	$x_{\mathrm{Pred.}}$	$x_{\mathrm{Exp.}}$	% error
1	46	2	19.0	17	11.8
2	92	2	19.2	23.5	18.3
3	110	7.5	32.7	35	6.6

5. Conclusions. – From the reported results, it can be concluded that: *1*) The proposed model and method to analyze the small-scale laboratory reactor results produce rate expressions that correspond to *intrinsic* kinetics, *i.e.*, independent of the reactor configuration. The obtained kinetic model is very simple and represents the laboratory information with good accuracy. *2*) When the large-reactor model is used *to predict* the reactor performance and the results are compared with experimental data, good agreement is observed. It confirms the validity of mathematical modeling for scaling up intrinsic results from a small laboratory reactor.

The authors are grateful to *Consejo Nacional de Investigaciones Científicas y Técnicas* (*CONICET*), Universidad Nacional del Litoral (UNL), *Agencia Nacional de Promoción Científica y Tecnológica* (ANPCyT), and *Programa de Modernización Tecnológica-SECyT-CONICET*, for their support to produce this work. They also thank Eng. *C. M. Romani* for technical assistance.

Appendix. – Consider *Eqn. 1*. Since the reactor content is well mixed, $\nabla \cdot \boldsymbol{N}_i = 0$. We can integrate the resulting equation in the system volume. The integral of the left-hand side can be divided in two volumes: the photoreactor volume (V_{R}) and the rest of the system volume ($V_{\mathrm{T}} - V_{\mathrm{R}}$). On the right-hand side, we can consider that there is reaction only in the reactor volume. Then *Eqn. A-1* holds. Since the volumes are fixed, we can interchange the derivative and the integral signs. On each of the resulting terms, we can apply the volume-

average theorem given in *Eqn. A-2*, in which $\langle\ \rangle$ stands for the volume averaged value. Dividing by V_T and rearranging, *Eqn. A-3* is obtained. The first term of the latter gives the difference between outlet and inlet concentrations in the reactor. If V_R/V_T is small and the conversion per pass is differential, this term will be negligible. If the system is well-mixed, the changes in concentrations in $V_T - V_R$ will be equal to the changes in concentrations in the tank. The final result is *Eqn. 5* in *Sect. 3.3*.

$$\int_{V_R} \frac{\partial C_i(t)}{\partial t} \mathrm{d}V + \int_{V_T - V_R} \frac{\partial C_i(t)}{\partial t} dV = \int_{V_R} R_{\mathrm{Hom},i,\lambda}\, \mathrm{d}V \tag{A-1}$$

$$V_R \frac{\partial}{\partial t} \langle C_i(t) \rangle_{V_R} + (V_T - V_R) \frac{\partial}{\partial t} \langle C_i(t) \rangle_{V_T - V_R} = V_R \langle R_{\mathrm{Hom},i,\lambda}(x,t) \rangle_{V_R} \tag{A-2}$$

$$\frac{V_R}{V_T} \frac{\partial}{\partial t} [\langle C_i(t) \rangle_{V_R} - \langle C_i(t) \rangle_{V_T - V_R}] + \frac{\partial}{\partial t} \langle C_i(t) \rangle_{V_T - V_R} = \frac{V_R}{V_T} \langle R_{\mathrm{Hom},i,\lambda}(x,t) \rangle_{V_R} \tag{A-3}$$

REFERENCES

[1] T. Matsuura, J. M. Smith, *AIChE J.* **1970**, *16*, 1064.
[2] Y. Ogata, K. Tomizawa, K. Takagi, *Can. J. Chem.* **1981**, *59*, 14.
[3] H. Kawaguchi, *Chemosphere* **1993**, *26*, 1965.
[4] M. Bideau, B. Claudel, M. Otterbein, *J. Photochem.* **1980**, *14*, 291.
[5] L. Davydov, P. Smirniotis, *J. Catal.* **2000**, *191*, 105.
[6] R. B. Bird, W. E. Stewart, E. L. Lightfoot, 'Transport Phenomena', J. Wiley & Sons, Inc., New York, 1960 p. 556 and 53.
[7] R. J. Brandi, O. M. Alfano, A. E. Cassano, *Environ. Sci. Technol.* **2000**, *34*, 2631.
[8] A. O. Allen, C. J. Hochanadel, J. A. Ghormley, T. W. Davis, *J. Phys. Chem.* **1952**, *56*, 575.
[9] O. M. Alfano, R. L. Romero, A. E. Cassano, *Chem. Eng. Sci.* **1985**, *40*, 2119.
[10] O. M. Alfano, R. L. Romero, A. E. Cassano, *Chem. Eng. Sci.* **1986**, *41*, 1155.
[11] O. M. Alfano, R. L. Romero, C. A. Negro, A. E. Cassano, *Chem. Eng. Sci.* **1986**, *41*, 1163.
[12] C. A. Martín, O. M. Alfano, A. E. Cassano, *Water Sci. Technol.* **2001**, *44(5)*, 53.
[13] C. A. Martín, O. M. Alfano, A. E. Cassano, *Catal. Today* **2000**, *60*, 119.
[14] G. V. Buxon, C. L. Greenstock, W. P. Helman, A. B. J. Ross, *Phys. Chem. Ref. Data* **1988**, *17*, 513.
[15] B. H. J. Bielski, D. E. Cabelli, R. L. Arudi, A. B. J. Ross, *Phys. Chem. Ref. Data* **1985**, *14*, 1041.
[16] M. I. Stefan, J. R. Bolton, *Environ. Sci. Technol.* **1998**, *32*, 1588.
[17] S. L. Murov, I. Carmichael, G. L. Hug, ' Handbook of Photochemistry', 2nd edn., Marcel Dekker, Inc., New York, 1993, p. 299.
[18] D. W. Marquardt, *J. Soc. Indust. Appl. Math.* **1963**, *11*, 431.
[19] A. E. Cassano, C. A. Martín, R. J. Brandi, O. M. Alfano, *Ind. Eng. Chem. Res.* **1995**, *34*, 2155.
[20] H. A. Irazoqui, J. Cerdá, A. E. Cassano, *AIChE J.* **1973**, *19*, 460.

Received May 30, 2001